Langmuir

Article

pubs.acs.org/Langmuir

Self-Organization of Quantum Rods Induced by Lipid Membrane Corrugations

Thomas Bizien,[†,‡,§] Jean-Claude Ameline,[‡] Kevin G. Yager,[∥] Valérie Marchi,[†] and Franck Artzner*[,‡]

[†]Université de Rennes 1, CNRS UMR 6226, Institut des Sciences Chimiques de Rennes, Avenue du Général Leclerc, 35042 Rennes, France

[‡]Université de Rennes 1, CNRS UMR 6251, Institut de Physique de Rennes, Avenue du Général Leclerc, 35042 Rennes, France

[§]Synchrotron SOLEIL l'Orme des Merisiers Saint-Aubin - BP 48 91192 Gif-sur-Yvette Cedex, France

[∥]Center for Functional Nanomaterials, Brookhaven National Laboratory, Upton, New York 11973, United States

Supporting Information

ABSTRACT: Self-organization of fluorescent nanoparticles, using biological molecules such as phospholipids to control assembly distances, is a promising method for creating hybrid nanostructures. We report here the formation of hybrid condensed phases made of anisotropic nanoparticles and phospholipids. Such structure formation is driven by electrostatic interaction between the nanoparticles and the phospholipids, and results in the formation of a 2D rectangular liquid crystal, as confirmed by high-resolution Small-Angle X-ray Scattering (SAXS). Moreover, we show that the fluorescent properties of the NPs are not modified by the self-assembly process.

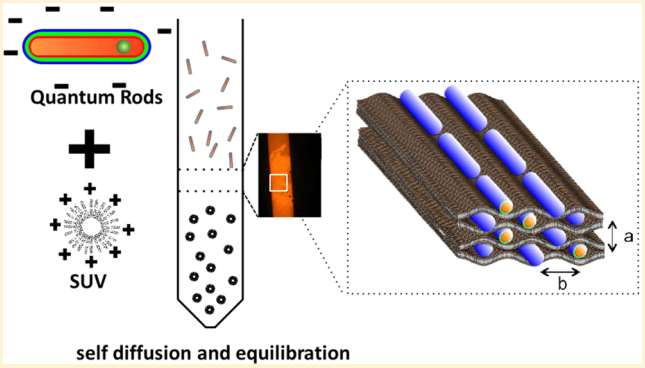

INTRODUCTION

Nanoparticle (NP) crystallization is a key challenge in the creation of materials bearing new and tunable properties, such as fluorescence, Raman enhancement, and phonon-plasmon coupling.[1−3] The main problems to overcome are the control of the crystal lattice and the interdistance between NPs. One route to this control is via DNA coronas to regulate assembly.[4−8] The crystallization can also be controlled using templates to direct assembly.[9−11] One elegant possibility is to use membranes with either NPs[12] or polyelectrolytes molecules such as DNA.[13] Cationic phospholipidic membrane interactions with anionic macromolecules are well-known and have been described in detail.[13−17] In those cases, the interaction is induced by electrostatic attraction between DNA and the membranes, resulting in the formation of liquid crystalline phases. Polymorphism was detected in those phases.[17] This polymorphism is present as well in the case of quantum dots (QDs) crystallizing within phospholipids membranes.[12] For those samples, hierarchical self-organization was obtained, but the structures were lacking long-range positional order. Adding a protein such as actin gave the possibility to introduce anisotropy and gave rise to long-range order in the system.[10,18]

We previously reported such a method by using a mixture of actins/phospholipids/quantum dots, which allowed 3D structuring over long distances. In this case, the conjugation of the components gave rise to membrane undulation, which thus tunes the interdistance between NPs.[10] An interesting possibility is the creation of long-range order without the use of a protein. Such a design would simplify the system and therefore ease the process of hybrid structure formation. Here, we report on the formation of ordered hybrid assemblies of rigid nanoparticles and phospholipid membranes. In order to induce anisotropy in such a system, we used semiconductor anisotropic NPs, known as quantum rods (QRs). We previously reported the synthesis and surface functionalization of QRs.[19] Due to their shape and their net negative surface charge, QRs can be used instead of DNA, as was previously demonstrated,[14] which strengthens the system. Phospholipidic systems are known to undergo phase transitions depending on the temperature. A specific phase transition known as the L_β-to-L_α transition ties in to the melting of the alkyl chains of the phospholipids; therefore, a decrease in the phospholipids thickness should be observed concomitantly.[20−22]

EXPERIMENT

Materials. Cadmium oxide (CdO, 99.998%), selenium (S, 99,5%), and hexylphosphonic acid (HPA, 99%) were purchased from Alfa Aesar. Sulfur (S, 99+%) was purchased from Strem Chemical. Trioctylphosphine oxide (TOPO, 99%), trioctylphosphine (TOP, 97%), octadecylphosphonic acid (ODPA, 97%) were purchased from Sigma-Aldrich. Peptides TCPAC (Figure 3b) was purchased from polypeptide laboratories France (purity, HPLC, 90+%). Dimyristoylphosphatidylcholine (DMPC) and dimyristoyltrimethylammonium-

Received: January 21, 2015
Revised: October 7, 2015
Published: October 15, 2015

ACS Publications © 2015 American Chemical Society

DOI: 10.1021/acs.langmuir.5b03335
Langmuir 2015, 31, 12148−12154

propane (DMTAP) were purchased from Avanti polar Lipids, Inc. All reagents were used as received.

QR Synthesis. We adapted the protocol of Carbone et al.[23] to our purpose. More precisely, CdSe/CdS nanorods were synthesized in two steps, as follows:

(1) To prepare the CdSe seeds, TOPO (3.0 g), ODPA (0.280 g), and CdO (0.060 g) were mixed in a 25 mL glass flask, heated to 150 °C under vacuum for 1 h. Then, under argon, the mixture temperature was increased to 320 °C in order to dissociate CdO. When the reddish solution turned clear and colorless, 1.5 g of TOP was injected in the flask, and the setting was changed to 350 °C. Upon reaching the latter temperature, 0.058 g of Se dissolved in 0.360 g of TOP were added. After 30 s, the solution turned orangish, and the heating mantel was removed to allow the flask to cool down to room temperature. The obtained solution of CdSe core was finally supplemented with 3 mL of TOP and stored until further use.

(2) To grow a CdS shell on the CdSe cores, CdO (0.031 g), TOPO (1.555 g), ODPA (0.150 g), and HPA (0.041 g) were mixed in a flask and heated at 150 °C under vacuum for 1 h. Under argon, the solution was next heated up to 350 °C to dissociate CdO. When it turned clear and colorless, 1.5 g of TOP was added, and the temperature was increased to 350 °C. Once this new temperature setting was reached, we quickly injected a solution, which had been prepared by diluting 0.062 g of sulfur in 0.775 g of TOP containing 200 μL of CdSe cores at 400 μM. The reaction was allowed to proceed for 10 min and was stopped by thermal quenching. The resulting fluorescent suspension was dissolved in 5 mL toluene and washed 3 times with 50 mL of a methanol: toluene (5:1) mixture, relying on cycles including centrifugation for 10 min at 3000 g supernatant removal and pellet redispersion in fresh solvent. Once the excess of ligands removed, 3 mL of pure toluene was used for the final storage (typically at 50 μM).

Peptide Grafting. Just before functionalization, the preceding hydrophobic QRs were washed three more times in a similar way, in order to remove all ligands remaining in solution. The final redispersion was achieved in chloroform so as to obtain 30 μL aliquots at 10 mg·mL^{-1}. The latter organic suspension was next mixed with 90 μL of 20 mM aqueous peptide solution, an addition followed by 5 μL of tetramethylammonium hydroxide (TMAOH) at 25% (w/w) in methanol. Transfer of the fluorescent particles from the organic phase to the aqueous one was then observed. After 15 min of incubation, chloroform was subsequently allowed to evaporate at room temperature for 0.5 h. Ligand excess was eventually removed by size exclusion chromatography using sephadex G-25 columns (NAP-5 or NAP-10 from GE Healthcare). Both column equilibration and elution were performed with ultrapure water.

Vesicles Preparation. (1) Large unilamellar vesicles (LUVs) were prepared by the extrusion method. Briefly, two batches were prepared either with a (DMPC/DMTAP) mixture (80:20) or with pure DMPC in chloroform. After solvent evaporation, an aqueous solution of 30 mM sucrose, 10 mM NaCl and 100 μM NaN_3 was added and the resulting suspension was successively put in a liquid nitrogen bath for 30 s and in a water bath at 40 °C for 30 s. The sequence was repeated five times. The obtained multilamellar vesicle (MLV) suspension was then extruded through a 100 nm polycarbonate filter (Extruder Avestin Inc., Ottawa, Ontario, Canada) and obtained at a concentration of 20 mg·mL^{-1}. The mean hydrodynamic diameter of the obtained LUVs was measured by dynamic light scattering (DLS) and found to be around 105 ± 15 nm for pure DMPC and 100 ± 17 nm for the DMPC/DMTAP mixture.

(2) Small unilamellar vesicles (SUVs) were prepared from a (DMPC/DMTAP) mixture (80:20) dissolved in chloroform. After solvent evaporation and drying under N_2 flow, the lipidic film was hydrated by ultrapure water at 50 °C at a concentration of 20 mg.mL^{-1} and then sonicated to clarity before use. SUVs size was estimated by DLS and found to be around 40 nm ±13 nm.

Characterization. *UV–Vis Absorption Spectroscopy.* Measurements were achieved using a Cary 100 SCAN UV–vis spectrometer (Varian) and 1 cm long quartz cuvettes. The concentration of QRs in the various suspensions was calculated as described in the literature, i.e., relying on the absorbance at 350 nm as well as on the corresponding nanorod absorption coefficient $\varepsilon_{350} = (0.38 \times 10^{26})V$ mol^{-1}, where V is the particle volume in cm^3.[24]

Fluorescence Spectroscopy. Emission spectra were recorded on a Fluorolog-3 fluorimeter (Horiba Jobin-Yvon). All samples were excited at their absorption maxima, which had previously been evaluated by UV–vis spectrometry. In addition, to avoid self-absorption effects the optical density at the excitation wavelength was set between 0.01 and 0.1.

Microspectro Fluorescence. Fluorescence spectra were acquired with an IX-71 Olympus inverted microscope modified as follow: a laser diode (405 nm, Cube-405, Coherent, California, USA) and a fibered spectrometer (Avaspec-2048, Avantes, The Netherlands) was centered behind the output port of the microscope. The spatial resolution was 25 μm (with the 4× objective), the spectral resolution was 1 nm.

DLS and Zeta Potential Measurements. The measurements of the mean hydrodynamic diameters were performed at an angle of 173° using a Nanosizer ZEN3600 (Malvern Instruments, England) and collected at 25 °C. All solutions were first diluted to micromolar concentration and then filtered through 0.2 μm Millipore filter (Millex HV, Sigma-Aldrich, France).

The colloid electrophoretic mobility and zeta potential measurements were performed using the Zetasizer ZEN3600 (Malvern Instruments, England) equipped with a He–Ne laser source (λ = 633 nm). The colloidal suspension of vesicles was loaded into disposable folded capillary cells Zeta Cell (DTS 1060) and data were collected at 25 °C. The colloids zeta potential and mobility were extracted from the inelastic frequency shift of the laser signal scattered by moving charged colloid under an electric field (applied cell voltage was 15 V).

Small Angle X-ray Scattering. Homemade setup: X-ray patterns were collected with a Pilatus 300 K (Dectris, Baden, Switzerland), mounted on a microsource X-ray generator GeniX 3D (Xenocs, Sassenage, France) operating at 30 W. The monochromatic CuK_α radiation is of λ = 1.541 Å. The diffraction patterns were therefore recorded for reciprocal spacing $q = 4\pi^* \sin\theta/\lambda$ in a range of repetitive distances from 0.015 Å^{-1} (418 Å) and 0.77 Å^{-1} (8 Å).

National Synchrotron Light Source (NSLS) at Brookhaven National Laboratory: High-resolution (HR) SAXS experiments were performed at the X9 beamline,[25] using X-rays of wavelength λ = 0.885 Å (14.0 keV). The diffraction patterns were recorded using a fiber-coupled CCD area detector, in the reciprocal-space range (real space repeat distance) of 0.004 Å^{-1} (1570 Å) to 0.14 Å^{-1} (45 Å).

RESULTS AND DISCUSSION

QR functionalization must allow the NPs to be water-soluble and stable in suspension to interact with cationic membranes. To do so, we designed a system so that QRs were functionalized with hydrophilic ligands bearing a negative charge and thus could be used as anionic particles.

To begin, QRs were synthesized as described by Manna's group.[23] We selected a batch of QRs with high monodispersity in length and diameter (Figure 1a) and with well-characterized optical properties (Figure 1b). This batch was functionalized[19] as we previously demonstrated with the TCPAC peptide giving anionic TCPAC-QRs (QRs−) (Figure 3b). First, the possible interaction between QRs− and phospholipidic vesicles was tested by Zeta potential measurements using a suspension of charged LUVs (0.2 mg·ml^{-1}) and adding small aliquots of QRs− (Figure 2).

As an inversion of charge was observed during the titration (Figure 2), a clear interaction between the LUVs and the QRs− through electrostatic forces is demonstrated. Then, in order to obtain phospholipidic lamellar phase, a mixture of 80:20 DMPC/DMTAP at higher concentration (20.0 mg mL^{-1}) was prepared and sonicated in Millipore water to generate cationic SUVs (SUV+) following well-known protocols.[10,12] TCPAC-QRs in large excess were added into X-ray glass capillaries

DOI: 10.1021/acs.langmuir.5b03335
Langmuir 2015, 31, 12148−12154

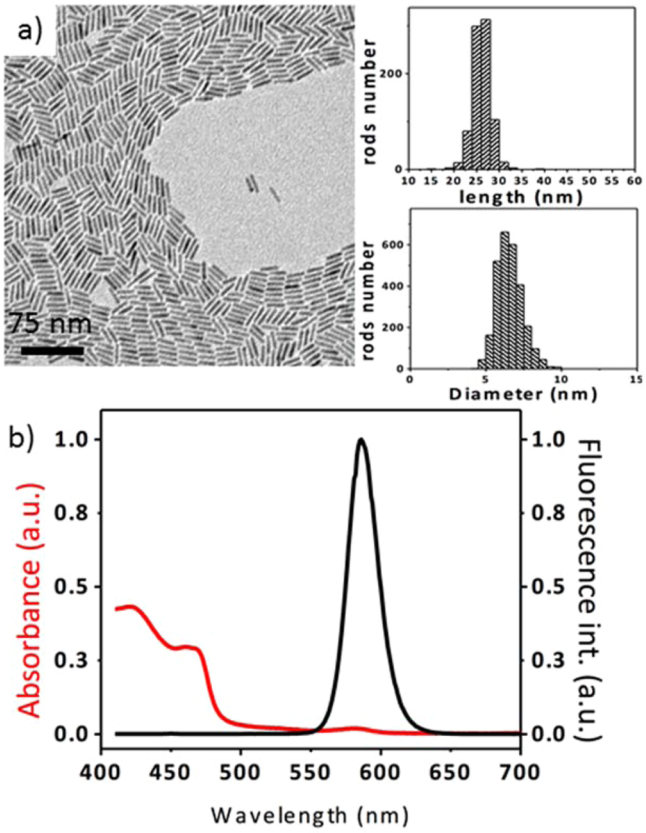

Figure 1. TEM image of the QR batch used in this paper and size (length and diameter) distribution showing QRs of 24 × 6 nm (a). Typical fluorescence spectrum (black line) and UV−visible absorption spectra (red line) of the synthesized QRs (b).

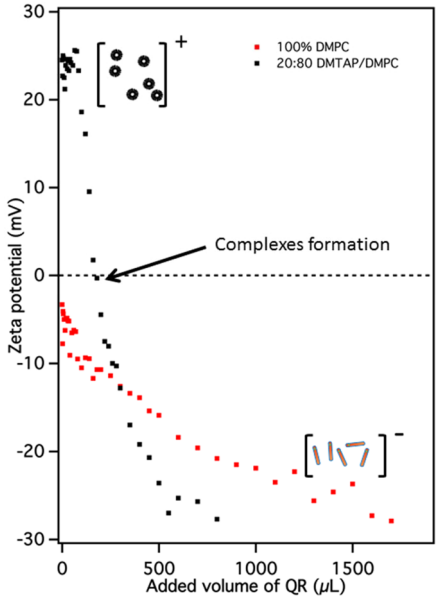

Figure 2. Zeta potential (ζ) as a function of the added volume of QRs− (2.5×10^{-8} M) during the titration of LUVs suspensions: DMPC/DMTAP mixture (80:20) (black square) and DMPC (red square). For the DMPC LUVs titration by QRs−, no charge inversion is observed, the zeta potential measurement is heading toward QRs− zeta potential (around −28 mV) . In the contrary, for the titration of LUVs+ by QRs−, a charge inversion is observed as more QRs− are added until reaching the QRs− zeta potential (−28 mV).

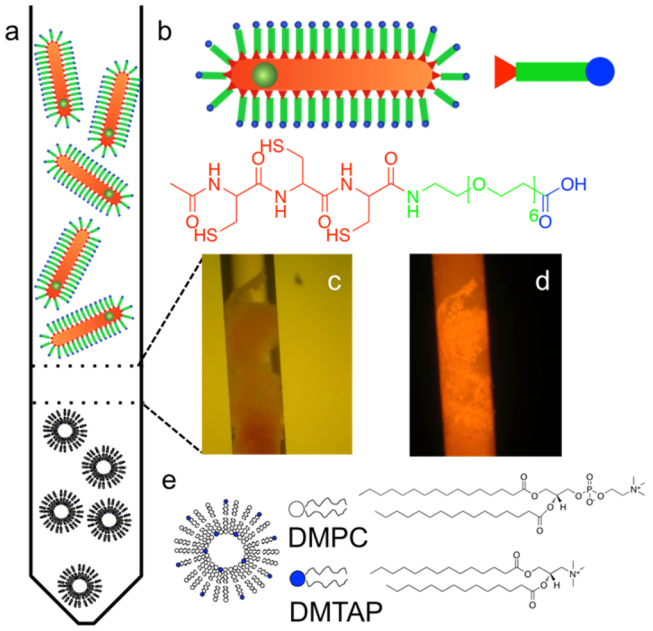

Figure 3. Sketch of the capillaries filled with QRs− and SUV+ (a). QRs are functionalized with the TCPAC peptide (b). Image of the obtained precipitate after a few day exhibiting: bright field (c) and (d) fluorescence. (e) Sketch of the prepared SUV+.

(diameter: 1.5 mm) previously filled with DMPC/DMTAP SUV+ (Figure 3a,b,e). The capillaries were held at room temperature for 48 h to allow self-diffusion of QRs− and SUV +. After 1 day, an orangey precipitate was observed in the capillaries (Figure 3c,d). The precipitates were run through temperature cycles (10 times): 30 min at 4 °C followed by 30 min at 50 °C, in order to equilibrate the resulting structure. The final assemblies were then left at room temperature for several days.

The X-ray experiments were carried out at the NSLS X9 beamline at Brookhaven National Laboratory for HR-SAXS, and on a homemade setup for the other patterns. The sample temperature was controlled within 0.1 °C using a water bath regulating system.

Small angle X-ray scattering (SAXS) is the ideal experimental technique for in situ investigation of the structuring of our hybrid samples. These materials are not easily studied by electron microscopy (TEM or STEM) owing to inevitable loss of structure during drying. The condensed three-dimensional ordering makes them unsuitable for surface probing via atomic force microscopy (AFM). SAXS is one of the only techniques that can resolve their nanoscale order in their native environment. The SAXS 2D data exhibit a set of distinct scattering rings. We then integrated the 2D image and obtained a 1D plot of the intensity versus q ($Å^{-1}$), q being a distance in the reciprocal space, $q = 2\pi/d$, d being the distance in the real space. We then observed the presence of both sharp and broad peaks (Figure 4a).

The sharp peaks were assigned to a multilamellar phase that can be indexed with a repeating distance d = 88 Å. This interdistance is larger than the one from pure phospholipids multilamellar structures ($d_{lamDMPC} \approx 44.2$ Å). Therefore, since $d > d_{lamDMPC}$, as it was observed for DNA (d = 65.1 Å),[15,17] QRs− are embedded within the phospholipidic layers. Moreover, the broader peaks correspond to a QRs superlattice in between phospholipidic layers. The peaks position can

DOI: 10.1021/acs.langmuir.5b03335
Langmuir 2015, 31, 12148−12154

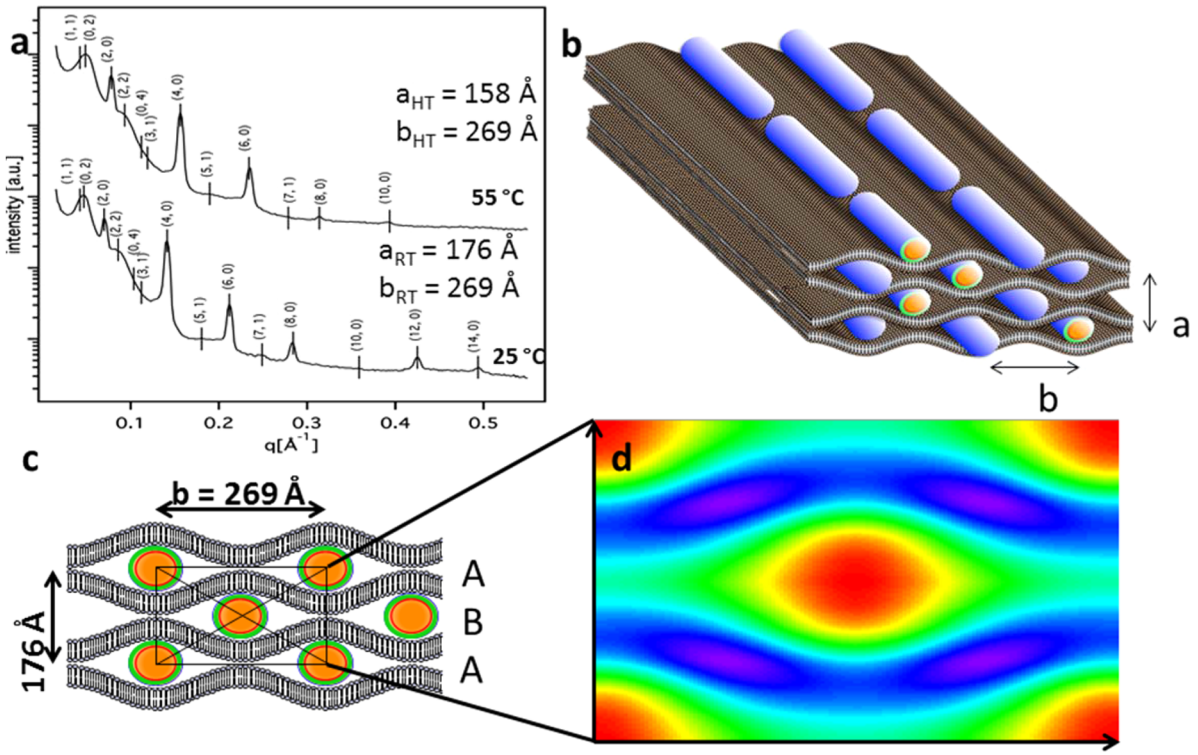

Figure 4. (a) SAXS pattern after radial integration of the QRs−/SUV+ superstructure obtained after equilibration at 25 °C (bottom) and at 55 °C (top) after chain melting using a temperature gradient. (b) 3D sketch of the obtained hybrid phase and (c) 2D sketch of the obtained phase and its electron density projection.

therefore be indexed (Table 1) as a rectangular centered QRs lattice $q_{h,k} = 2\pi(a^{*2} \times h^2 + b^{*2} \times k^2)^{1/2}$ with $a^* = 2\pi/a$ and $b^* = 2\pi/b$, a and b being the 2D lattice constants, the systematic missing of (h, k) peaks with $h + k = 2n + 1$ demonstrate the centered symmetry. The centered rectangular symmetry is built around oriented planar QRs lattice, $a = 2d = 176$ Å is fixed by the interdistance between two phospholipids bilayer, $b = 269$ Å is fixed by the interdistance between coplanar QRs. The QRs are displaced into an ABAB configuration in alternating layers, which gives rise to the centered phase.

Table 1. Indexing of SAXS Patterns from Figure 4a at 25°C RT Using the Following Parameters: a = 176 Å and b = 269 Å[a]

RT (25 °C)			
(h, k)	q_{th} (Å)	q_{exp} (Å)	F_{obs}
(1,1)	0.0425	0.0412	20
(0,2)	0.0469	0.0468	5
(2, 0)	**0.0709**	**0.0709**	**25**
(2,2)	0.0851	0.0857	−3
(0,4)	0.0939	0.1024	+ 0.002
(3, 1)	0.109	0.1117	−5
(4, 0)	**0.1494**	**0.1414**	**2**
(5, 1)	0.1789	0.1803	
(6, 0)	**0.2118**	**0.2118**	**1**
(7, 1)	0.2494	0.2489	
(8, 0)	**0.2837**	**0.2842**	**+ 0.5**
(10, 0)	**0.3547**	**0.3584**	**+ 0.005**
(12, 0)	**0.4256**	**0.4251**	**+ 0.3**
(14, 0)	**0.4965**	**0.494**	**+ 0.2**

[a]The bolded data correspond to the lamellar peaks.

A model of the obtained phase is proposed in Figure 4b,c. Indeed, the simple sum of two phospholipidic bilayers and QRs− thickness $a = 2d_{lam} = 2d_{QR} + 2e_{lip}$ is not compatible with the distance found, a being equal to 176 Å and not 272 Å; e_{lip} being approximately equal to 40 Å[22] and d_{QR} = 96 Å. The simple possibility to reduce the distance between two membranes is to induce undulation of the surface and that the QRs are embedded within the same lipid membrane. If such an undulation occurs, the new lamellar thickness should be $a = d = d_{QR} + 2e_{lip}$, and a is then equal to 176 Å. This supports our hypothesis. This was previously shown in the case of QD[12] and QD + actin filaments.[10]

In order to check this proposed structure, lipid chain melting experiment were performed (from 25 to 55 °C). Interestingly, only the sharp peaks are affected by the temperature increase (Figure 5). The melting process occurs from 30 to 38 °C with a gradual disappearance of the L_β peak and the L_α peak gradually appearing. The full SAXS curve of the new melted phase is showed in Figure 5.

The melting temperature is found to be around 34 °C. First, we can see that the structure is conserved on the SAXS spectra. Thus, we present in Table 2 an indexing for the new phase. As for the room temperature experiment, the peak positions are indexed as a centered rectangular lattice. a_{HT} and b_{HT} being the 2D lattice constant, a_{HT} is the new interdistance between two phospholipidic bilayers and is equal to 158 Å and b_{HT} to 269 Å. An 18 Å decrease corresponding to two times the decrease of the membranes thickness from the L_β phase to the L_α phase was observed for all of the lamellar peaks. This thickness decrease is only due to the phospholipids alkyl chains melting process. Nevertheless, the QRs interdistance does not change. Thus, the QRs remain well assembled in both possible phases of the soft membrane component.

DOI: 10.1021/acs.langmuir.5b03335
Langmuir 2015, 31, 12148−12154

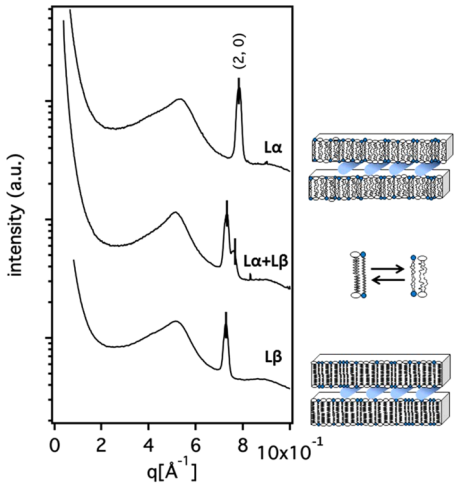

Figure 5. HRSAXS of the lipids chains melting experiment, exhibiting a phase transition from the L_β to the L_α phase around 34 °C. Sketches show the crystallized lipids chains, the equilibrium between melted and crystallized chains, and the melted chains.

Table 2. Indexation of SAXS Patterns from Figure 4a at 55°C HT Using the Following Parameters: a = 158 Å and b = 269 Å[a]

HT (55 °C)		
(h, k)	q_{th} (Å)	q_{exp} (Å)
(1, 1)	0.0425	0.0445
(0, 2)	0.0469	0.0487
(2, 0)	**0.0786**	**0.0782**
(2, 2)	0.0916	0.0932
(0, 4)	0.0939	0.0972
(3, 1)	0.1203	0.1192
(4, 0)	**0.1572**	**0.1563**
(5, 1)	0.1980	0.1896
(6, 0)	**0.2359**	**0.2341**
(7, 1)	0.2763	0.2787
(8, 0)	**0.3146**	**0.3139**
(10, 0)	**0.3932**	**0.3936**

[a]The bolded data correspond to the lamellar peaks.

In the case of the DNA-cationic lipid complexes, the DNA-interdistance increase through the L_β-L_α transition because of electrostatic neutrality.[26] Indeed, the increase of lipid area reduces the surface charge of the membranes, and the DNA rods charge is constant. When the membranes are planar, such as in the case of the DNA, the polyelectrolyte interdistance has to increase in order to satisfy the electroneutrality.[26] In the case of lipid complexes of rods, the membranes are hugely corrugated, and the amplitude or the shape of the corrugation is another solution for the system to fulfill the electroneutrality.

The proposed model (Figure 4b,c) exhibits corrugated phospholipidic layers induced by the strong electrostatic affinity between the anionic QR− and the cationic SUV+. The repeating distance is the sum of the half of a QR (QR+ligands) diameter and of two phospholipids bilayers. QD are known to induce such phases, as well as DNA and actin.[10,12,17,15] The energy needed to deform the membrane increases as l^{-4} (l being the deformation wavelength),[27] as QRs− used in this paper presented a diameter of about 9.6 nm, the deformation energy required to deform the membrane should be roughly reduced by a factor of $(9.6/2.0)^4 = 530$. Those undulations are thus not forbidden. Their maximal amplitudes are about a QR half diameter, e.g., 4.8 nm.

In order to get better detail of those undulations, electron density (ED) was calculated from SAXS data. This projection should provide us an insight of the corrugated phases.[10,20] Thanks to the large number of observed peaks at 25 °C (Figure 4a) the electron density projection shown in (Figure 4d) was calculated using the following formula:

$$\rho_{(x,y)} = \sum_{h,k} F_{(h,k)} \cos(2\pi xh + 2\pi yk) \quad (1)$$

where $F_{(h,k)}$, the structure factors of the unit cell, are complex numbers. Their arguments are related to the observed intensity of each (h,k) peak.

$$I_{(h,k)} = |F_{(h,k)}|^2 \quad (2)$$

Unfortunately, however, the phases cannot be measured by X-ray scattering. Due to the centro-symmetry of the *cmm* rectangular structure, the phase is either 0 or π. $F_{(h,k)}$ are consequently real number, positive or negative. In order to solve the phase problem (the sign problem in our case), the n phase can be deduced from molecular assumptions on the electronic density profiles of the 2D unit cell. Indeed most of the sign sequence will generate reconstructed electronic densities which are not in agreement with the expected organization. The sign choice is based on three criteria: QRs must be centered at the origin, the phospholipidic membrane had to be continuous, oscillating and presenting a quasi-constant electronic density, and finally we compared e_{lam} (interdistance between the center of the electron density projection of the lamellar phases) to previously obtained values (50 to 55 Å).[14,28] The choice was realized following three steps: first, only one solution among the 2^4 solutions corresponding to the four strongest $F_{(h,k)}$ peaks were phased. Then the three medium $F_{(h,k)}$ peaks were phased. And finally the weakest peaks were phased. The unique projection that respects those criteria is shown in Figure 4c. All the others ED showed a lack of oscillation, or continuity in the ED of the phospholipidic membrane, or a wrong e_{lip} membrane width. Some inappropriate electron density reconstructions are shown as Supporting Information. It is noteworthy that the observed 2D organization is due to the formation of QR chains that are embedded within the same corrugation line (Figure 4b).

A key challenge is to obtain new properties in assembled nanomaterial due to NPs crystallization with a controlled lattice symmetry and spacing. The use of fluorescent NPs, as here, should lead to materials bearing new emission properties. Various effects have been previously observed in such dense phases of fluorescent nanoparticles. In some cases, the close distances between emitting dipoles generate a quenching of the NPs fluorescence.[29] On the other hand, stimulated light emission can be observed.[30−34] The parameters that govern the fluorescence properties should be the NP interdistances as well as the 3D NPs organizations. Indeed NP interdistances strongly affect the mode of fluorescence coupling: at short distances, the overlapping of wave functions allows tunneling energy transfer, which is the source of either quenching or FRET. At longer distances, only electromagnetic coupling is possible, thereby generating superradiance.[35−37] The superradiance coupling is coherent and proportional to the positional pair correlation function:

DOI: 10.1021/acs.langmuir.5b03335
Langmuir 2015, 31, 12148−12154

$$\Gamma(\vec{k} - \vec{k}_0) = \left| \frac{1}{N} \sum_{l=1}^{N} e^{i(\vec{k}-\vec{k}_0)\cdot\vec{r}_l} \right|^2 \quad (3)$$

Interestingly, the fluorescence intensity depends upon the position of the emitting dipoles, and is exalted by a 3D crystalline order.[10]

Fluorescence properties were investigated upon laser excitation of the samples. Fluorescence emission spectra were recorded at three distinct positions in the same capillaries we used for SAXS measurement (Figure 6). The first measurement

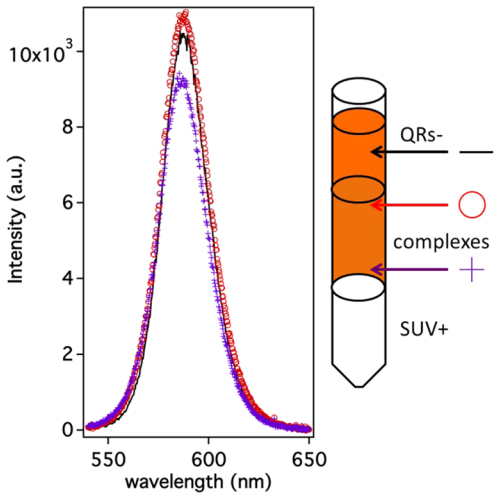

Figure 6. Fluorescence spectrum in the same capillary of the QRs− suspension (plain line), in the bottom (purple cross) and at the top of the formed structures (red circles) inside of the capillary showing no modification of the fluorescence properties.

was acquired in the QRs− solution, away from the precipitate, in order to obtain a precise measure of the QRs− fluorescent emission properties (wavelength and intensity). Then we recorded the spectra at two different positions within the precipitate. Comparing the spectra recorded within the same sample, a slight difference in the fluorescence intensity was observed, but no modification of the wavelength maxima was detected. Thereafter, we compared the previous spectra to the one corresponding to the QRs− solution. Again we observed a slight difference in emission intensities but there was no modification of the wavelength maxima. No quenching of the QR− fluorescence is observed after the self-organization process in contrast with other self-organization process. But superradiance is not observed, which confirms the need of a 3D order to reach this particular coupling mode.[10]

In this paper, we have proved that a superstructure is formed through self-organization due to the strong interaction between the QRs− and the SUV+. The 2D superstructure was found as a centered rectangular phase. The structure is robust with temperature and not disturbed by melting of the phospholipid chains. It is interesting to note that this assembly strategy provides a QR interdistance that is much larger than what can be formed using only molecular ligands and drying.[25] Thus, it is possible through templating to tune the interdistance between NPs. Moreover we showed that there is no alteration of the QR optical properties after this self-organization.

■ ASSOCIATED CONTENT

Supporting Information

The Supporting Information is available free of charge on the ACS Publications website at DOI: 10.1021/acs.langmuir.5b03335.

Supporting figures (PDF)

■ AUTHOR INFORMATION

Corresponding Author

*E-mail: franck.artzner@univ-rennes1.fr.

Notes

The authors declare no competing financial interest.

■ ACKNOWLEDGMENTS

F.A. and V.M. thank the Region Bretagne for TB Ph.D. fellowship. F.A. aknowledges FEDER for financial support. We would like to thank Chiara Coronna for the first X-ray experiments. This research used resources of the Center for Functional Nanomaterials (CFN), and the National Synchrotron Light Source (NSLS), which are U.S. DOE Office of Science Facilities, at Brookhaven National Laboratory (BNL), supported under Contract No. DE-SC0012704. CFN and BNL are acknowledged for guest fellowships.

■ REFERENCES

(1) Grzelczak, M.; Vermant, J.; Furst, E. M.; Liz-Marzán, L. M. Directed Self-Assembly of Nanoparticles. *ACS Nano* **2010**, *4* (7), 3591−3605.

(2) Alvarez-Puebla, R. n. A.; Agarwal, A.; Manna, P.; Khanal, B. P.; Aldeanueva-Potel, P.; Carbo-Argibay, E.; Pazos-Pérez, N.; Vigderman, L.; Zubarev, E. R.; Kotov, N. A.; Liz-Marzàn, L. M. Gold nanorods 3D-supercrystals as surface enhanced Raman scattering spectroscopy substrates for the rapid detection of scrambled prions. *Proc. Natl. Acad. Sci. U. S. A.* **2011**, *108* (20), 8157−8161.

(3) Wang, W.; Vasa, P.; Pomraenke, R.; Vogelgesang, R.; De Sio, A.; Sommer, E.; Maiuri, M.; Manzoni, C.; Cerullo, G.; Lienau, C. Interplay between Strong Coupling and Radiative Damping of Excitons and Surface Plasmon Polaritons in Hybrid Nanostructures. *ACS Nano* **2014**, *8*, 1056.

(4) Nykypanchuk, D.; Maye, M. M.; van der Lelie, D.; Gang, O. DNA-guided crystallization of colloidal nanoparticles. *Nature* **2008**, *451* (7178), 549−552.

(5) Xiong, H.; Sfeir, M. Y.; Gang, O. Assembly, Structure and Optical Response of Three-Dimensional Dynamically Tunable Multicomponent Superlattices. *Nano Lett.* **2010**, *10* (11), 4456−4462.

(6) Xiong, H.; van der Lelie, D.; Gang, O. DNA Linker-Mediated Crystallization of Nanocolloids. *J. Am. Chem. Soc.* **2008**, *130* (8), 2442−2443.

(7) Macfarlane, R. J.; Lee, B.; Jones, M. R.; Harris, N.; Schatz, G. C.; Mirkin, C. A. Nanoparticle Superlattice Engineering with DNA. *Science* **2011**, *334* (6053), 204−208.

(8) Caruso, F., Ed. *Colloids and Colloid Assemblies:Synthesis, Modification, Organization and Utilization of Colloid Particles* ; Wiley-VCH Verlag GmbH & Co. KGaA: Weinheim, Germany, 2004.

(9) Liang, H.; Angelini, T. E.; Braun, P. V.; Wong, G. C. L. Roles of Anionic and Cationic Template Components in Biomineralization of CdS Nanorods Using Self-Assembled DNA−Membrane Complexes. *J. Am. Chem. Soc.* **2004**, *126* (43), 14157−14165.

(10) Henry, E.; Dif, A.; Schmutz, M.; Legoff, L.; Amblard, F.; Marchi-Artzner, V.; Artzner, F. Crystallization of Fluorescent Quantum Dots within a Three-Dimensional Bio-Organic Template of Actin Filaments and Lipid Membranes. *Nano Lett.* **2011**, *11* (12), 5443−5448.

(11) Yang, L.; Liang, H.; Angelini, T. E.; Butler, J.; Coridan, R.; Tang, J. X.; Wong, G. C. L. Self-assembled virus-membrane complexes. *Nat. Mater.* **2004**, *3* (9), 615−619.

DOI: 10.1021/acs.langmuir.5b03335
Langmuir 2015, 31, 12148−12154

(12) Dif, A.; Henry, E.; Artzner, F.; Baudy-Floc'h, M.; Schmutz, M.; Dahan, M.; Marchi-Artzner, V. Interaction between Water-Soluble Peptidic CdSe/ZnS Nanocrystals and Membranes: Formation of Hybrid Vesicles and Condensed Lamellar Phases. *J. Am. Chem. Soc.* **2008**, *130* (26), 8289−8296.
(13) Artzner, F.; Zantl, R.; Rapp, G.; Rädler, J. O. Observation of a Rectangular Columnar Phase in Condensed Lamellar Cationic Lipid-DNA Complexes. *Phys. Rev. Lett.* **1998**, *81* (22), 5015−5018.
(14) Zantl, R.; Baicu, L.; Artzner, F.; Sprenger, I.; Rapp, G.; Rädler, J. O. Thermotropic Phase Behavior of Cationic Lipid-DNA Complexes Compared to Binary Lipid Mixtures. *J. Phys. Chem. B* **1999**, *103* (46), 10300−10310.
(15) Rädler, J. O.; Koltover, I.; Salditt, T.; Safinya, C. R. Structure of DNA-Cationic Liposome Complexes: DNA Intercalation in Multilamellar Membranes in Distinct Interhelical Packing Regimes. *Science* **1997**, *275* (5301), 810−814.
(16) Caracciolo, G.; Pozzi, D.; Caminiti, R.; Mancini, G.; Luciani, P.; Amenitsch, H. Observation of a Rectangular DNA Superlattice in the Liquid-Crystalline Phase of Cationic Lipid/DNA Complexes. *J. Am. Chem. Soc.* **2007**, *129* (33), 10092−10093.
(17) Koltover, I.; Salditt, T.; Rädler, J. O.; Safinya, C. R. An inverted hexagonal phase of cationic liposome-DNA complexes related to DNA release and delivery. *Science* **1998**, *281*, 78−81.
(18) Caillé, A.; Artzner, F.; Amblard, F. Ordered Stacking of F-Actin Layers and Mixed Lipid Bilayers: A Columnar Liquid Crystal. *Phys. Rev. Lett.* **2013**, *110* (4), 048102.
(19) Bizien, T.; Even-Hernandez, P.; Postic, M.; Mazari, E.; Chevance, S.; Bondon, A.; Hamon, C.; Troadec, D.; Largeau, L.; Dupuis, C.; Gosse, C.; Artzner, F.; Marchi, V. Peptidic Ligands to Control the Three-Dimensional Self-Assembly of Quantum Rods in Aqueous Media. *Small* **2014**, *10* (18), 3707−3716.
(20) Luzzati, V.; Tardieu, A.; Gulik-Krzywicki, T.; Rivas, E.; Reiss-Husson, F. Structure of the Cubic Phases of Lipid-Water Systems. *Nature* **1968**, *220* (5166), 485−488.
(21) Petrache, H. I.; Tristram-Nagle, S.; Nagle, J. F. Fluid phase structure of EPC and DMPC bilayers. *Chem. Phys. Lipids* **1998**, *95* (1), 83−94.
(22) Tristram-Nagle, S.; Liu, Y.; Legleiter, J.; Nagle, J. F. Structure of Gel Phase DMPC Determined by X-Ray Diffraction. *Biophys. J.* **2002**, *83* (6), 3324−3335.
(23) Carbone, L.; Nobile, C.; De Giorgi, M.; Sala, F. D.; Morello, G.; Pompa, P.; Hytch, M.; Snoeck, E.; Fiore, A.; Franchini, I. R.; Nadasan, M.; Silvestre, A. F.; Chiodo, L.; Kudera, S.; Cingolani, R.; Krahne, R.; Manna, L. Synthesis and Micrometer-Scale Assembly of Colloidal CdSe/CdS Nanorods Prepared by a Seeded Growth Approach. *Nano Lett.* **2007**, *7* (10), 2942−2950.
(24) Alam, R.; Fontaine, D. M.; Branchini, B. R.; Maye, M. M. Designing Quantum Rods for Optimized Energy Transfer with Firefly Luciferase Enzymes. *Nano Lett.* **2012**, *12* (6), 3251−3256.
(25) Zhang, Y. G.; Lu, F.; Yager, K. G.; van der Lelie, D.; Gang, O. A general strategy for the DNA-mediated self-assembly of functional nanoparticles into heterogeneous systems. *Nat. Nanotechnol.* **2013**, *8*, 865−872.
(26) Zantl, R.; Artzner, F.; Rapp, G.; Rädler, J. O. Thermotropic structural changes of saturated-cationic-lipid DNA complexes. *EPL (Europhysics Letters)* **1999**, *45* (1), 90.
(27) de Gennes, P. G.; Prost, J. *The Physics of Liquid Crystals*; Oxford Science Publications: Oxford, U.K., 1995.
(28) Hauet, N.; Artzner, F.; Boucher, F.; Grabielle-Madelmont, C.; Cloutier, I.; Keller, G.; Lesieur, P.; Durand, D.; Paternostre, M. Interaction between Artificial Membranes and Enflurane, a General Volatile Anesthetic: DPPC-Enflurane Interaction. *Biophys. J.* **2003**, *84* (5), 3123−3137.
(29) Tang, Z.; Ozturk, B.; Wang, Y.; Kotov, N. A. Simple Preparation Strategy and One-Dimensional Energy Transfer in CdTe Nanoparticle Chains. *J. Phys. Chem. B* **2004**, *108* (22), 6927−6931.
(30) Kazes, M.; Lewis, D. Y.; Banin, U. Method for Preparation of Semiconductor Quantum-Rod Lasers in a Cylindrical Microcavity. *Adv. Funct. Mater.* **2004**, *14* (10), 957−962.
(31) Kazes, M.; Lewis, D. Y.; Ebenstein, Y.; Mokari, T.; Banin, U. Lasing from Semiconductor Quantum Rods in a Cylindrical Microcavity. *Adv. Mater.* **2002**, *14* (4), 317−321.
(32) Lupo, M. G.; Della Sala, F.; Carbone, L.; Zavelani-Rossi, M.; Fiore, A.; Lüer, L.; Polli, D.; Cingolani, R.; Manna, L.; Lanzani, G. Ultrafast Electron Hole Dynamics in Core/Shell CdSe/CdS Dot/Rod Nanocrystals. *Nano Lett.* **2008**, *8* (12), 4582−4587.
(33) Zavelani-Rossi, M.; Lupo, M. G.; Krahne, R.; Manna, L.; Lanzani, G. Lasing in self-assembled microcavities of CdSe/CdS core/shell colloidal quantum rods. *Nanoscale* **2010**, *2* (6), 931−935.
(34) Zavelani-Rossi, M.; Krahne, R.; Della Valle, G.; Longhi, S.; Franchini, I. R.; Girardo, S.; Scotognella, F.; Pisignano, D.; Manna, L.; Lanzani, G.; Tassone, F. Self-assembled CdSe/CdS nanorod microlasers fabricated from solution by capillary jet deposition. *Laser & Photonics Reviews* **2012**, *6* (5), 678−683.
(35) Scheibner, M.; Schmidt, T.; Worschech, L.; Forchel, A.; Bacher, G.; Passow, T.; Hommel, D. Superradiance of quantum dots. *Nat. Phys.* **2007**, *3* (2), 106−110.
(36) Dicke, R. H. Coherence in Spontaneous Radiation Processes. *Phys. Rev.* **1954**, *93* (1), 99−110.
(37) Duncan, A.; Stehle, P. Superradiance: A numerical study. *Phys. Rev. A: At., Mol., Opt. Phys.* **1987**, *35* (10), 4181−4185.

DOI: 10.1021/acs.langmuir.5b03335
Langmuir 2015, 31, 12148−12154